Equatorial wave structure of the Madden-Julian Oscillation

Jialin Lin[1], Minghua Zhang[2] and Brian Mapes[1]

[1] **NOAA-CIRES Climate Diagnostics Center, Boulder, CO 80305**
[2] **State University of New York, Stony Brook, NY 11794**

January, 2003

ABSTRACT

A Kelvin-wave conceptual model has often been used in studying wave-convection feedbacks in the Madden-Julian Oscillation (MJO). This study examines whether the equatorial wave structure of the MJO is similar to a pure Kelvin wave, using long term observations from tropical sounding stations and NCEP reanalysis, supplemented by measurements from the Tropical Ocean Global Atmosphere (TOGA) Coupled Ocean Atmosphere Response Experiment. All datasets are filtered using a 30-70 day bandpass filter. The long-term MJO composites are constructed using linear correlation and linear regression with respect to surface precipitation.

Consistent with the observed top-heavy heating profile, the wave structure has a deep inflow layer in the lower troposphere and an outflow layer near the tropopause. In the upper layer, there are strong Rossby gyres in the subtropics. The wave structure along the equator is different from the pure Kelvin wave, in that the geopotential height lags the zonal wind by nearly a quarter cycle. Implications of the observed wave structure for the wave-convection feedback mechanisms are discussed.

1. Introduction

Discovered by Madden and Julian (1971, 1972), the Madden-Julian Oscillation (MJO) is the dominant intraseasonal mode in tropical convection and circulation (e.g. Weickmann et al. 1985, Lau and Chan 1985, Salby and Hendon 1994, Wheeler and Kiladis 1998). It affects a wide range of tropical weather such as the onset and breaks of the Indian and Australian summer monsoons (e.g. Yasunari 1979, Hendon and Liebmann 1990), and the formation of tropical cyclones (e.g. Nakazawa 1986, Liebmann et al. 1994). It also drives teleconnections to the extratropics (e.g., Lau and Phillips 1986) and impacts some important extratropical weather. On a longer timescale, the MJO is observed to trigger or terminate some El Nino events (e.g. Kessler et al. 1995, Takayabu et al. 1999, Bergman et al. 2001). Therefore, the MJO is important for both extended-range weather forecasting and long-term climate prediction.

A Kelvin-wave conceptual model has often been used in studying the wave-convection feedback mechanisms in the MJO, such as the wave-CISK (Convective Instability of the Second Kind) mechanism (e.g. Takahashi 1987, Chang and Lim 1988, Lim et al. 1990, Crum and Dunkerton 1992), the frictional wave-CISK mechanism (e.g. Wang 1988, Moskowitz and Bretherton 2000), the WISHE (Wave Induced Surface Heat Exchange) mechanism (e.g. Emanuel 1987, Neelin et al. 1987, Crum and Dunkerton 1994), the phase-lagged wave-CISK mechanism (e.g. Cho et al. 1994), and the phase-lagged WISHE mechanism (e.g. Emanual 1993, Neelin and Yu 1994, Yu and Neelin 1994, Goswami and Rao 1994). The usage of a Kelvin-wave model was justified by the

following characteristics of the MJO from the early observations (Madden and Julian 1971, 1972, Parker 1973): (1) the eastward propagation, (2) the absence of large amplitude in the meridional wind component near the equator, (3) the absence of Rossby gyres at low levels. Later observational studies (e.g. Weickmann et al. 1985, Knutson and Weickmann 1987, Rui and Wang 1990, Salby and Hendon 1994) showed that the upper level wind structure of the MJO has Rossby gyres in the subtropics, but the wind structure along the equator still shows the first two characteristics, which are similar to the Kelvin wave.

However, another characteristic of the Kelvin wave, which is important for wave-convection feedback, is the in-phase relationship between zonal wind and geopotential height. Only a few observational studies analysed the phase relation between zonal wind and geopotential height (or temperature) in the MJO (Hendon and Salby 1994, Kiladis and Weickmann 1992, Hsu 1996), and they showed inconsistent results.

Hendon and Salby (1994) constructed the composite life cycle of the MJO using temperature from the MSU channel 2 and wind from a four-dimensional assimilation product. They found that as the MJO moves eastward from the western Indian Ocean to the central Pacific Ocean, the MSU channel 2 temperature is always nearly in phase with the 200 mb zonal wind. Assuming that the geopotential height has a simple baroclinic structure along the equator and the MSU channel 2 temperature represents the troposphere mean temperature, the 200 mb geopotential height would also be in phase with the 200 mb zonal wind. This is similar to the Kelvin wave.

On the contrary, Kiladis and Weickmann (1992) and Hsu (1996) constructed the

composite life cycle of the MJO using wind and geopotential height data both from the four-dimensional assimilation. They found that over the western Pacific Ocean, the 200 mb geopotential height lags the zonal wind by a quarter cycle. This is different from the Kelvin wave.

The motivation of this study is to use the in situ sounding data to check which of the above two results is correct. Madden and Julian (1971, 1972, 1994) and Nishi (1989) used the sounding data to calculate the phase difference between the zonal wind and the geopotential height. As reviewed by Madden and Julian (1994), the results are complex. Their method is somehow different from the above three papers (Hendon and Salby 1994, Kiladis and Weickmann 1992, Hsu 1996) which used deep convection as the reference time series. In order to compare with the results of Hendon and Salby (1994), Kiladis and Weickmann (1992), and Hsu (1996), in this study we use deep convection as the reference time series.

The datasets used in this study are described in section 2. Methods are described in section 3. The observed MJO wave structure is described in section 4. Implications of the observed wave structure for the wave-convection feedback mechanisms are discussed in section 5, and summary is given in section 6.

2. Data

The datasets used include long-term data and TOGA COARE data.

The long term datasets cover 21 years from 1979 to 1999. They include:

(1) The upper air sounding from the tropical stations (Fig. 1). The variables used

include wind, geopotential height and temperature at 12 mandatory levels. We average the data at each station to pentad data. There are only a few missing data. They are filled with linear interpolation.

(2) The daily NCEP reanalysis data. The variables used include upper air wind, geopotential height, temperature and specific humidity, and surface latent and sensible heat fluxes. The horizontal resolution is 2.5 degree longitude by 2.5 degree latitude. We average the data along the equator (between 5N and 5S) to pentad data with a zonal resolution of 10 degree longitude.

(3) The pentad NCEP Chi-corrected divergence and vertical motion profiles calculated by Sardeshmukh et al. (1999). The horizontal resolution is 2.5 degree longitude by 2.5 degree latitude. We average the data along the equator (between 5N and 5S) with a zonal resolution of 10 degree longitude. This data is dynamically consistent diabatic heating derived from twice-daily NCEP reanalyses. See Sardesmukh et al. (1999) for details of the technique.

(4) The pentad CMAP precipitation calculated by Xie and Arkin (1997). The horizontal resolution is 2.5 degree longitude by 2.5 degree latitude. We average the data along the equator (between 5N and 5S) with a zonal resolution of 5 degree longitude.

The TOGA COARE datasets cover 120 day from November 1, 1992 to Feburary 28, 1993. They include:

(1) the 6-hourly IFA sounding array budgets calculated by Ciesilski et al. (2002),

(2) the daily OSA sounding array budgets calculated by us using the method of Zhang and Lin (1997), and

(3) the 3-hourly IFA surface precipitation, latent heat flux and sensible heat flux calculated by Curry et al. (2001).

3. Method

All datasets are filtered using a 30-70 day Murakami (1976) filter, whose response function is shown in Fig. 2. The central frequency correspond to a period of 45 day. The half amplitude is at periods of 30 day and 70 day.

For the TOGA COARE data, there are two MJO events (see e.g. Chen et al 1996). We focus on the December 1992 event which is stronger and has better data availability. The maximum of the 30-70 day bandpass filtered precipitation anomaly at the location of the COARE measurements is at December 19, 1992.

For the long term data, an MJO composite is constructed using linear regression with respect to an MJO index. In this study, we use filtered CMAP precipitation as our MJO index. Because the MJO is a large-scale phenomenon dominated by wavenumber 0-6 (Wheeler and Kiladis 1998), the CMAP precipitation has been zonally filtered to keep only wavenumber 0-6. The confidence level of linear correlation is estimated following Oort and Yienger (1996).

4. Observed wave structure of the MJO

4.1 Vertical structure along the equator

Fig. 3 shows the vertical structure of MJO at 0N155E from 21 years of NCEP reanalysis data. The time lag is with respect to the time of maximum precipitation.

The time evolution is from the right to the left, showing the local evolution of measured variables as the eastward-moving MJO passes the measurement longitude. The zonal wind (Fig. 3a) shows a simple two-layer structure with the upper layer out of phase with the lower layer. The zonal wind in the upper layer leads the precipitation by nearly a quarter cycle.

This two-layer structure is well-known from many previous observations (e.g. Madden and Julian 1971, 1972, Weickmann et al. 1985, Knutzson and Weickmann 1987). An interesting feature which did not bring much attention is that the maxima of both the two layers are at a very high altitude, not the 850 mb and 200 mb levels used in many previous MJO studies. The maximum of the lower layer is around 600 mb (just below the 0 C level), while that of the upper layer is around 150 mb (just below the tropopause). It means that at the time of maximum precipitation, the zonal inflow is just below the 0 C level, and the zonal outflow is just below the tropopause. Consistent with this inflow-outflow feature, the vertical motion (Fig. 3b) concentrates in the upper troposphere. For clarity, the two-dimensional flow is plotted using arrows in Fig. 3c. This middle troposphere inflow and near tropopause outflow structure are consistent with the top-heavy heating profile shown in Lin et al. (2002).

The vertical motion shows a westward phase tilt with height. It develops first in the lower troposphere, and then shifts upward as it intensifies. This westward phase tilt of vertical motion is consistent with the westward phase tilt of the associated heating anomaly shown in Lin et al. (2002), and may reflect or indicate more shallow

convection in the earlier stage, and more stratiform precipitation in the later stage.

The geopotential height (contours in Fig. 3c) also shows a two-layer structure, with the upper layer out of phase with the lower layer. The node is also at high level around 350 mb, as high as that of the zonal wind. Th geopotential height in the upper layer is nearly in phase with the precipitation.

Notice the phase difference between the geopotential height and the zonal wind, which is a key indicator of the wave type. At the upper layer, the geopotential height lags the zonal wind by a quarter cycle. Because for both the zonal wind and the geopotential height the upper layer is out of phase with the lower layer, at the lower layer, the geopotential height also lags the zonal wind by a quarter cycle. This quarter cycle phase difference indicates that the equatorial wave structure of the MJO is not a Kelvin wave.

In summary, the equatorial wave structure of the MJO in the NCEP reanalysis has three characteristics: (1) The flow is middle-troposphere inflow and near tropopause outflow at the time of maximum precipitation. (2) The vertical motion has a westward phase tilt with height. (3) The zonal wind lags the geopotential height by a quarter cycle.

The quarter cycle phase difference is consistent with the results of Kiladis and Weickmann (1992) and Hsu (1996) using the operational analysis data, but inconsistent with the result of Hendon and Salby (1994) using the MSU channel 2 temperature data. Therefore next we use the in situ sounding data to validate the above results. Fig. 4 is the same as Fig. 3 except for the MJO event observed by TOGA COARE

Outer Sounding Array (OSA). The zonal wind (Fig. 4a), vertical motion (Fig. 4b), and geopotential height (Fig. 4c) all look similar to the NCEP reanalysis composite in Fig. 3, showing the three characteristics listed above. An MJO composite of 21 years of sounding data at Pohnpei (Fig. 5) also supports the NCEP reanalysis composite, especially the quarter cycle phase difference between the zonal wind and the geopotential height. Further analysis of the sounding data from other stations (Chuuk, Honiara) gives similar results (not shown). Therefore the in situ sounding data support the NCEP reanalysis composite and the results of Kiladis and Weickmann (1992) and Hsu (1996), but does not support the result of Hendon and Salby (1994).

Why does the MSU channel 2 temperature used by Hendon and Salby (1994) give different result? The answer lies in the vertical structure of the temperature anomaly in the MJO (Fig. 6). Consistent with the geopotential height anomaly (Fig. 3c, Fig. 4c, Fig. 5b), the temperature anomaly concentrates in the upper troposphere, and is nearly in phase with the precipitation and upward motion. The temperature anomaly in the lower troposphere is very small, and tends to lead that in the upper troposphere. The MSU channel 2 temperature used in Hendon and Salby (1994) has most of its weighting from the lower and middle troposphere (Spencer et al. 1990, their Fig. 1). Therefore, the MSU channel 2 is not suitable for representing the troposphere mean temperature in the MJO.

We do not have access to the MSU channel 2 temperature data, but we have obtained a new version of the MSU temperature which seperates the upper troposphere

temperature (called MSU34) and the lower troposphere temperature (called MSU23). The weighting function of MSU channel 2 temperature is similar to that of MSU23. Fig. 7 shows the MJO composite of (a) MSU34 and (b) MSU23 at 0N155E. We can see that MSU34 nearly in phase with the precipitation, which is consistent with the upper troposphere temperature in the sounding data. MSU23 leads the precipitation by more than a quarter cycle, which is similar to the lower troposphere temperature in the sounding data. Therefore, MSU34 is better in representing the upper troposphere temperature anomaly in the MJO.

4.2 Horizontal structure

In the previous subsection, we have demonstrated that along the equator both the zonal wind and the geopotential height have a two-layer structure, with the center of the upper layer at 150 mb for both the zonal wind and the geopotential height, and the center of the lower layer at 700 mb for the zonal wind. To put the vertical structure along the equator in a three-dimensional perspective, next we look at the horizontal wave structure at these two layers. Fig. 8 shows the horizontal pattern of the geopotential height anomaly at 150 mb and 700 mb. For clarity, we plot the component symmetric to the equator. The most significant feature of the upper layer wave structure (Fig. 8a) is the strong Rossby gyres in the subtropics, The amplitude of Z anomaly at the centers of the Rossby gyres is four times as large as the maximum amplitude of Z anomaly along the equator. The centers of the anticyclones lag the equatorial precipitation by nearly a quarter cycle, i.e., the precipitation lies at

the node between the anticyclones and the cyclones. We'll discuss about these strong Rossby gyres later in section 5. At the lower layer (Fig. 8b), there is no strong Rossby gyre.

4.3 Schematics of the observed wave structure

Fig. 9 shows the schematics of the observed MJO wave structure. It has the following characteristics:

(1) At the time of maximum precipitation, the inflow is at the middle troposphere and the outflow is near the tropopause.

(2) The vertical motion has a westward phase tilt with height.

(3) The equatorial wave structure is different from the Kelvin wave, in that the geopotential height lags the zonal wind by a quarter cycle.

(4) The horizontal wave structure in the upper layer has very strong subtropical Rossby gyres.

5. Implications for wave-convection feedback

As discussed in the introduction, a Kelvin-wave conceptual model has often been used in studying wave-convection feedback in the MJO. The above results show that the observed equatorial wave structure is different from a pure Kelvin wave. How much does the difference affect the inferred wave-convection feedback processes?

Historically, different types of wave-convection feedback mechanisms emphasized different convective heating terms. With the aid of the column-integrated moisture

budget and neglecting horizontal eddy fluxes, the column-integrated convective heating can be written as (Yanai and Johnson 1993):

$$\begin{aligned}\int_{p_t}^{p_s} Q_c dp &= LP + S \\ &= \int_{p_t}^{p_b} (-L \bigtriangledown \cdot \overline{q}\,\overline{\mathbf{v}})\, dp \; + \int_{p_b}^{p_s} (-L \bigtriangledown \cdot \overline{q}\,\overline{\mathbf{v}})\, dp \\ &\quad + (LE + S) \; + \int_{p_t}^{p_s} (-L \frac{\partial \overline{q}}{\partial t})\, dp \end{aligned} \tag{1}$$

where Q_c is the convective heating, p_t is the tropopause pressure, p_s the surface pressure, p_b the pressure at the top of the boundary layer, L the latent heat of vaporization, P is the surface precipitation, S the surface sensible heat flux, q the mixing ratio of water vapor, $\mathbf{v}$ the horizontal velocity, ω the vertical velocity, and E the surface evaporation rate. $\bigtriangledown$ is the isobaric del operator. The overbar denotes the running horizontal average. The first term in Eq. 1 is the free troposphere moisture convergence. The second term is the boundary layer moisture convergence. The third term is the surface heat flux. The last term is the column-integrated local drying of moisture. These four terms have been emphasized by the wave-CISK mechanism, the frictional wave-CISK mechanism, the WISHE mechanism, and the charge-discharge mechanism, respectively.

Fig. 10 shows these four heating terms during the life cycle of the MJO during TOGA COARE. The free troposphere moisture convergence (Fig. 10a) is nearly in phase with the precipitation, which is as expected because it is the dominant term in the moisture budget. The boundary layer troposphere moisture convergence (Fig. 10b) leads the precipitation by nearly a quarter cycle, which is consistent with

previous observations (e.g. Hendon and Slaby 1994). The surface heat flux (Fig. 10c) lags the precipitation by about 0.1 cycle, which is also consistent with previous observations (Jones and Weare 1996, Hendon and Glick 1997, Shinoda et al. 1998). The local drying of moisture (Fig. 10d) lags the precipitation by nearly a quarter cycle, which is again consistent with previous observations (Maloney and Hartmann 1998, Kemball-Cook and Weare 2001).

One key question for any given wave-convection feedback mechanism is the phase relationship between the heating term it emphasizes and the temperature anomaly. If they are in phase, the heating term tends to make the temperature anomaly amplify. If they are in quadrature, the heating term will contribute to horizontal propagation. As noted above, the equatorial temperature anomaly in the observed MJO wave structure is shifted westward for a quarter cycle compared with a pure Kelvin wave. This changes the phase relations between the temperature and the heating terms and therefore significantly affects the feedback mechanisms.

The wave-CISK mechanism (e.g. Hayashi 1970, Lindzen 1974, Lau and Peng 1987, Takahashi 1987, Chang and Lim 1988, Lim et al. 1990, Crum and Dunkerton 1992, Zhang and Geller 1994) emphasizes the free troposphere moisture convergence. In the Kelvin wave model, the free troposphere moisture convergence lags the temperature by nearly a quarter cycle (Fig. 11a). It could amplify the wave only when the wave has a westward tilt with height. In the observed MJO, the temperature anomaly is in phase with the free troposphere moisture convergence (Fig. 12a). Therefore the free troposphere moisture convergence contributes an in-phase tendency to the equatorial

temperature anomaly, without requiring a westward phase tilt of the wave.

The frictional wave-CISK mechanism (e.g. Hayashi 1971, Wang 1988, Rui and Wang 1990, Salby et al. 1994, Moskowitz and Bretherton 2000) emphasizes the boundary layer moisture convergence. In the Kelvin wave model, the boundary layer moisture convergence is nearly in phase with the temperature (Fig. 11b). In the observed MJO, the boundary layer moisture convergence leads the temperature by nearly a quarter cycle (Fig. 12b), contributing more of an eastward propagation tendency or pre-moistening of the lower troposphere rather than amplification to the temperature anomaly.

The WISHE mechanism (e.g. Emanuel 1987, Neelin et al. 1987, Crum and Dunkerton 1994) emphysizes the surface latent and sensible heat flux. In the original WISHE theory, the mean surface wind is assumed to be easterly, which makes the anomalous surface wind speed, and therefore the surface heat flux in phase with the surface easterly (the dashed line in Fig. 11c). Then in the Kelvin wave model, the surface heat flux is in phase with the temperature anomaly and amplifies the wave. However, later observational studies (e.g. Zhang 1996, Lin and Johnson 1996, Jones and Weare 1996, Shinoda et al. 1998) show that the surface heat flux is nearly in phase with the surface westerly (the solid line in Fig. 11c). In the Kelvin wave model, this means that the surface heat flux is out of phase with the temperature anomaly and damps the wave, an apparent shortcoming of the WISHE mechanism for explaining the existance of the MJO. However, in the observed MJO, the surface heat flux has positive correlation with the temperature anomaly (Fig. 12c), and therefore

amplifies the wave.

The charge-discharge mechanism (Blade and Hartmann 1993) considered the local variation of moisture in addition to the column-integrated moisture convergence and the surface heat flux. They proposed that the convective heating exists only when the upper air relative humidity is above a certain threshold value. The relative humidity threshold for deep convection makes the upper air moisture nearly in phase with the large-scale forcing. This mechanism has been investigated by many authors (e.g. Hayashi and Sumi 1986, Hayashi and Golder 1986, 1997, Lau et al. 1988, Itoh 1989, Raymond and Torres 1998, Wang and Shleshinger 1999), and is also called the "saturation triggering" by Hayashi and Golder (1997), and "preconditioning" by Raymond and Torres (1998). In this paper we will call it "charge-discharge" following Blade and Hartmann (1993) because this name emphasizes both the moistening before the deep convection and the drying after it. The phase-lagged wave-CISK mechanism (Hayashi 1971b, Kuo 1975, Cho et al. 1994), and the phase-lagged WISHE mechanism (Emanuel 1993, Neelin and Yu 1994, Goswami and Rao 1994) prescribe a difference between the large-scale forcing (the sum of the column-integrated moisture convergence and the surface heat flux) and the convective heating. This is equavalent to adding a third heating term whose phase is similar to that of the local drying of moisture.

In the Kelvin wave model, the local drying of moisture is nearly out of phase with the temperature and damps the wave (Fig. 11d). In the observed MJO, the local drying of moisture lags the temperature by a quarter cycle (Fig. 12c) and therefore

neither amplifies nor damps the temperature anomaly.

In summary, the westward phase shift of the temperature anomaly in the observed MJO wave structure relative to the theoretical Kelvin wave significantly affects the wave-convection feedback mechanisms. In the WISHE case, even the sign of the feedback is reversed. Therefore, the Kelvin wave conceptual model may not be appropriate for studying the wave-convection feedback mechanisms in the MJO, although it is useful for studying the observed convectively coupled Kelvin wave (Wheeler and Kiladis 1998, Wheeler et al. 1999, Straub and Kiladis 2002).

This observational study does not provide any explanation as to why the observed equatorial wave structure of the MJO is different from the pure Kelvin wave. However, one hint comes from the similarity between the observed horizontal wave structure (Fig. 8) and the well-known Matsuno-Gill pattern (Matsuno 1966, his Fig. 9, Gill 1980, his Fig. 1). Matsuno and Gill found that the circulation response to a heating source symmetric to the equator is a Kelvin-Rossby wave with a Kelvin wave component to the east of the heating and a Rossby wave component to the west of the heating. The geopotential height anomaly along the equator lags the zonal wind anomaly by nearly a quarter cycle. This is caused by the Rossby wave component to the west of the heating which shifts the equatorial geopotential height anomaly westward. In Matsuno (1966) and Gill (1980), the heating source is stationary, which does not directly correspond to the eastward moving MJO. Chao (1987) and Yamagata (1987) generalize the Gill model to moving heating source to simulate the MJO. They found that the solution is still the Matsuno-Gill pattern with a Kelvin wave

component to the east of the heating and a Rossby wave component to the west of the heating (see Figs. 4, 6, 7 of Chao 1987). These simple modeling studies provide a hint that the Rossby wave component forced by the heating source may be one candidate for making the equatorial wave structure of the MJO different from the pure Kelvin wave. The observed horizontal wave structure (Fig. 8) suggests that the Rossby wave component is indeed very strong in the real world.

6. Summary

A Kelvin-wave conceptual model has often been used in studying wave-convection feedback in the MJO. Our examination of the MJO wave structure using long-term in situ sounding data suggests that the observed wave structure along the equator is different from the pure Kelvin wave, in that the geopotential height lags the zonal wind by nearly a quarter cycle. This coincides with strong upper level Rossby gyres in the subtropics.

It is shown that the westward phase shift of the temperature anomaly in the observed MJO wave structure relative to the theoretical Kelvin wave significantly affects the wave-convection feedback mechanisms. In the WISHE case, even the sign of the feedback is reversed. Therefore, the Kelvin wave conceptual model may not be approporiate for studying the wave-convection feedback mechanisms in the MJO, although it is useful for studying the observed convectively coupled Kelvin wave.

REFERENCES

Bergman, J. W., H. H. Hendon, K. M. Weickmann, 2001: Intraseasonal Air-Sea Interactions at the Onset of El Nino. *Journal of Climate*, 14, 1702-1719.

Chao, W. C., 1987: On the origin of the tropical intraseasonal oscillation. *J. Atmos. Sci.*, **44**, 1940-1949; Corrigendum, 45, 1283.

Chen, S. S., R. A. Houze., and B. E. Mapes, 1996: Multiscale variability of deep convection in relation to large-scale circulation in TOGA COARE. *J. Atmos. Sci.*, 53, 1380-1409.

Gill, A. E., 1980: Some simple solutions for heat-induced tropical circulation. *Quart. J. Roy. Meteor. Soc.*, **106**, 447-462

Hayashi, Y., and A. Sumi, 1986: The 30-40 day oscillation simulated in an "aqua planet" model. *J. Meteor. Soc. Japan.*, 64, 451-466.

Hayashi, Y., and D. G. Golder, 1993: Tropical 40-50 and 25-30-day oscillations appearing in realistic and idealized GFDL climate models and the ECMWF dataset. *J. Atmos. Sci.*, 50, 464-494.

Hayashi, Y., and S. Miyahara, 1987: A three-dimensional linear response model of the tropical intraseasonal oscillation. *J. Meteor. Soc. Japan*, 65, 843-857.

Hendon, H. H., and B. Liebmann, 1990: A composite study of onset of the Australia monsoon. *J. Atmos. Sci.*, 47, 2227-2240.

Hendon, H. H., and M. L. Salby, 1994: The life cycle of the Madden-Julian oscillation. *J. Atmos. Sci.*, 51, 2225-2237.

Hendon, H. H., and M. L. Salby, 1996: Planetary-scale interactions forced by intraseasonal variations of observed convection. *J. Atmos. Sci.*, 53, 1751-1758.

Hsu, H.-H., 1996: Global view of the intraseasonal oscillation during northern winter. *J. Climate*, **9**, 2386-2406.

Itoh, H., 1989: The mechanism for the scale selection of tropical intraseasonal oscillations. Part I: Selection of wavenumber 1 and the three-scale structure. *J. Atmos. Sci.*, 46, 1779-1798.

Kessler, W. S., and M. J. McPhaden, and K. M. Weickmann, 1995: Forcing of intraseasonal Kelvin waves in the equatorial Pacific. *J. Geophys. Res.*, 100, 10613-10631.

Kiladis, G. N., and K. M. Weickmann, 1992: Circulation anomalies associated with tropical convection during northern winter. *Mon. Wea. Rev.*, **120**, 1900-1923.

Knutson, T. R., and K. M. Weickmann, 1987: The 30-60 day atmospheric oscillation: Composite life cycles of convection and circulation anomalies. *Mon. Wea. Rev.*, **115**, 1407-1436.

Lau, K.-M., and T. J. Phillips, 1986: Coherent fluctuations of extratropical geopotential height and tropical convection in intraseasonal timescales. *J. Atmos. Sci.*, 43, 1164-1181.

Lau, N. C., I. M. Held, and J. D. Neelin, 1988: The Madden-Julian oscillations in an idealized general circulation model. *J. Atmos. Sci.*, **45**, 3810-3831.

Liebmann, B., H. H. Hendon, and J. D. Glick, 1994: The relationship between t tropical cyclones of the western Pacific and Indian Oceans and the Madden-Julian oscillation. *J. Meteor. Soc. Japan*, 72, 401-411.

Madden, R. A., and P. R. Julian, 1971: Detection of a 40-50 day oscillation in the zonal wind in the tropical Pacific. *J. Atmos. Sci.*, **28**, 702-708.

Madden, R. A., and P. R. Julian, 1972: Description of global-scale circulation cells in the tropics with a 40-50 day period. *J. Atmos. Sci.*, **29**, 1109-1123.

Madden, R. A., and P. R. Julian, 1994: Observations of the 40-50-day oscillation -A review. *Mon. Wea. Rev.*, **122**, 814-837.

Matsuno, T., 1966: Quasi-geostrophic motions in the equatorial area. *J. Meteor. Soc. Japan*, 44, 25-43.

Murakami, M., 1979: Large-scale aspects of deep convective activity over the GATE area. *Mon. Wea. Rev.*, **107**, 994-1013.

Murakami, T., and T. Nakazawa, 1985: Tropical 45 day oscillation during the 1979 Northern Hemisphere summer. *J. Atmos. Sci.*, 42, 1107-1122.

Nishi, N., 1989: Observational study on the 30-60 day variations in the geopotential and temperature fields in the equatorial region. *J. Meteor. Soc. Japan*, **67**, 187-203.

Oort, A. H., and J. J. Yienger, 1996: Observed long-term variability in the Hadley circulation and its connection to ENSO. *J. Climate*, 9, 2751-2767.

Parker, D., 1973: Equatorial Kelvin waves at 100 millibars. *Quart. J. Roy. Meteor. Soc.*, **99**, 116-129.

Rui, H., and B. Wang, 1990: Development characteristics and dynamic structure of tropical intraseasonal convection anomalies. *J. Atmos. Sci.*, **47**, 357-379.

Salby, M. L., and H. H. Hendon, 1994: Intraseasonal behavior of clouds, temperature, and motion in the Tropics. *J. Atmos. Sci.*, **51**, 2207-2224.

Salby, M. L., R. B. Garcia, and H. H. Hendon, 1994: Planetary-scale circulations in the presence of climatological and wave-induced heating. *J. Atmos. Sci.*, **51**, 2344-2367.

Sardeshmukh, P. D., M. Newman, and C. R. Winkler, 1999: Dynamically consistent estimates of diabatic heating. Proceedings, 24th Climate Diagnostics and Prediction Workshop, Tucson, AZ, 172-175.

Spencer, R. W., J. R. Christy, and N. C. Grody, 1990: Global atmospheric temperature monitoring with satellite microwave measurements: Method and results 1979-84. *J. Climate*, **3**, 1111-1128.

Takayabu, Y .N., Toshio Iguchi, Misako Kachi, Akira Shibata and Hiroshi Kanzawa, 1999: Abrupt termination of the 1997-98 El Nino in response to a Madden-Julian oscillation. *Nature*, 402, 279-282.

Wang, W., and M. E. Schlesinger, 1999: The dependence on convection parameterization of the tropical intraseasonal oscillation simulated by the 11-layer UIUC atmospheric GCM. *J. Climate*, **12**, 1423-1457.

Weickmann, K. M., G. R. Lussky, and J. E. Kutzbach, 1985: Intraseasonal (30-60 day) fluctuations of outgoing longwave radiation and 250 mb streamfunction during northern winter. *Mon. Wea. Rev.*, 113, 941-961.

Wheeler, M., and G. N. Kiladis, 1999: Convectively coupled equatorial waves: Analysis of clouds and temperature in the wavenumber-frequency domain. *J. Atmos. Sci.*, **56**, 374-399.

Xie, P., and P. A. Arkin, 1997: Global precipitation: A 17-year monthly analysis based on gauge observations, satellite estimates, and numerical model outputs. *Bull. Amer. Meteor. Soc.*, **78**, 2539-2558.

Yamagata, T., 1987. A simple moist model relevant to the origin of intraseasonal distur-

bances in the tropics. *J. Meteor. Soc. Japan*, **65**, 153-165.

Yanai, M., B. Chen, and W.-W. Tung, 2000: The Madden-Julian oscillation observed during the TOGA COARE IOP: Global view. *J. Atmos. Sci., 57*, 2374-2396.

Yasunari, T., 1979: Cloudiness fluctuations associated with the northern hemisphere summer monsoon. *J. Meteor. Soc. Japan*, 57, 227-242.

Zhang, M. H., and M. A. Geller, 1994: Selective excitation of tropical atmospheric waves in wave-CISK: The effect of vertical wind shear. *J. Atmos. Sci.*, **51**, 353-368.

Zhang, M. H., and J. L. Lin, 1997: Constrained variational analysis of sounding data based on column-integrated budgets of mass, heat, moisture, and momentum: Approach and application to ARM measurements. *J. Atmos. Sci.*, **54**, 1503-1524.

FIGURE CAPTIONS

Fig. 1 Standard deviation of the 30-70 day bandpass filtered anomaly of the CMAP precipitation from 1979-1999. The unit is mm/day. The thick solid polygons are the sounding arrays during TOGA COARE. The inner one is the Intensive Flux Array (IFA). The outer one is the Outer Sounding Array (OSA).

Fig. 2 The response function of the Murakami filter used in this study.

Fig. 3 The vertical structure of the MJO anomaly for (a) zonal wind (m/s), (b) vertical velocity (mb/hr), and (c) geopotential height (m) for the 21 years (1979-1999) of NCEP reanalysis data at 0N155E. Negative values are shaded. The arrows in (c) are the wind vectors whose horizontal component is the zonal wind, and vertical component the vertical velocity.

Fig. 4 Same as Fig. 3 except for the TOGA COARE OSA data.

Fig. 5 Same as Fig. 3a, b except for the sounding data at Pohnpei.

Fig. 6 The vertical structure of the MJO temperature anomaly for (a) 21 years (1979-1999) of NCEP reanalysis data at 0N155E, (b) TOGA COARE OSA, and (c) 21 years (1979-1999) of upper air sounding data at Pohnpei.

Fig. 7 The temperature anomaly during the life cycle of the MJO for 15 years (1979-1993) of (a) MSU34 data, and (b) MSU23 data at 0N155E.

Fig. 8 The horizontal structure of the MJO anomaly for geopotential height (contours) and wind (vectors) at (a) 150 mb, and (b) 700 mb. Only the component symmetric to the equator is plotted.

Fig. 9 Schematic depiction of the observed MJO wave structure. The middle part of each panel represents the structure in the equatorial vertical plane. Regions of enhanced large-scale convection are indicated schematically by the clouds. The dark shading inside the clouds represents the maximum of the diabatic heating. The arrows represent the anomalous wind. "H" and "L" represent the high and low geopotential height anomalies, respectively. "W" inside thick solid circle and "C" inside thick dashed circle represent the warm and cold temperature anomalies, respectively. The upper part of each panel is a plan view of the wave at 150 mb centered at the equator. The contours represent the anomalous geopotential height. The arrows represent the anomalous wind. Shading indicates the positive heating anomaly. The lower part of each panel is the same as the upper part except for 700 mb.

Fig. 10 The anomaly during the life cycle of the TOGA COARE MJO event for (a) the free troposphere moisture convergence, (b) the boundary layer moisture convergence, (c) the surface heat flux (latent plus sensible), and (d) the local moisture storage.

Fig. 11 Schematic depiction of the wave-convection feedback for the moist Kelvin wave. Regions of enhanced large-scale convection are indicated schematically by the clouds. The dark shading inside the clouds represents the maximum of the diabatic heating. The arrows represent the anomalous wind. "H" and "L" represent the high and low geopotential height anomalies, respectively. "W" inside thick solid circle and "C" inside thick dashed circle represent the warm and cold temperature anomalies, respectively. The solid and dashed squares represent the convergence and divergence

anomalies, respectively. See text for further explanation.

Fig. 12 Same as Fig. 11 except for the observed MJO wave.

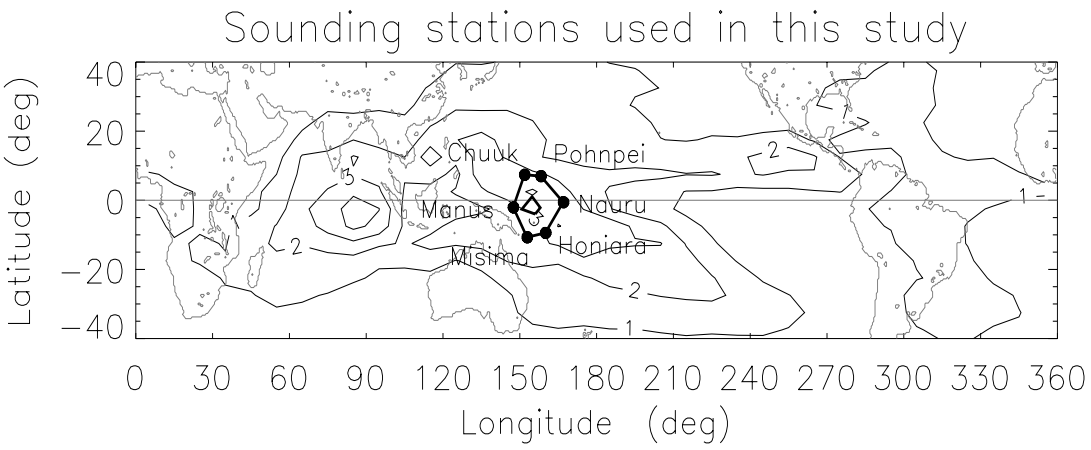
Sounding stations used in this study
Latitude (deg)
40
20
0
−20
−40
0
30
60
90
120
150
180
210
240
270
300
330
360
Longitude (deg)
Chuuk
Pohnpei
Manus
Nauru
Honiara
Misima
1
2
3
4
5

Figure 1:

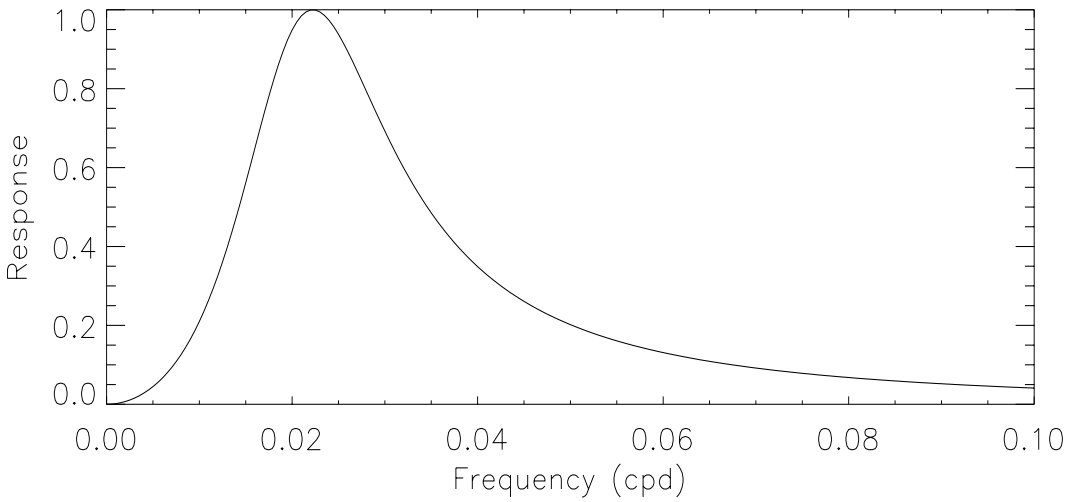
1.0
0.8
0.6
0.4
0.2
0.0
Response
0.00
0.02
0.04
0.06
0.08
0.10
Frequency (cpd)

Figure 2:

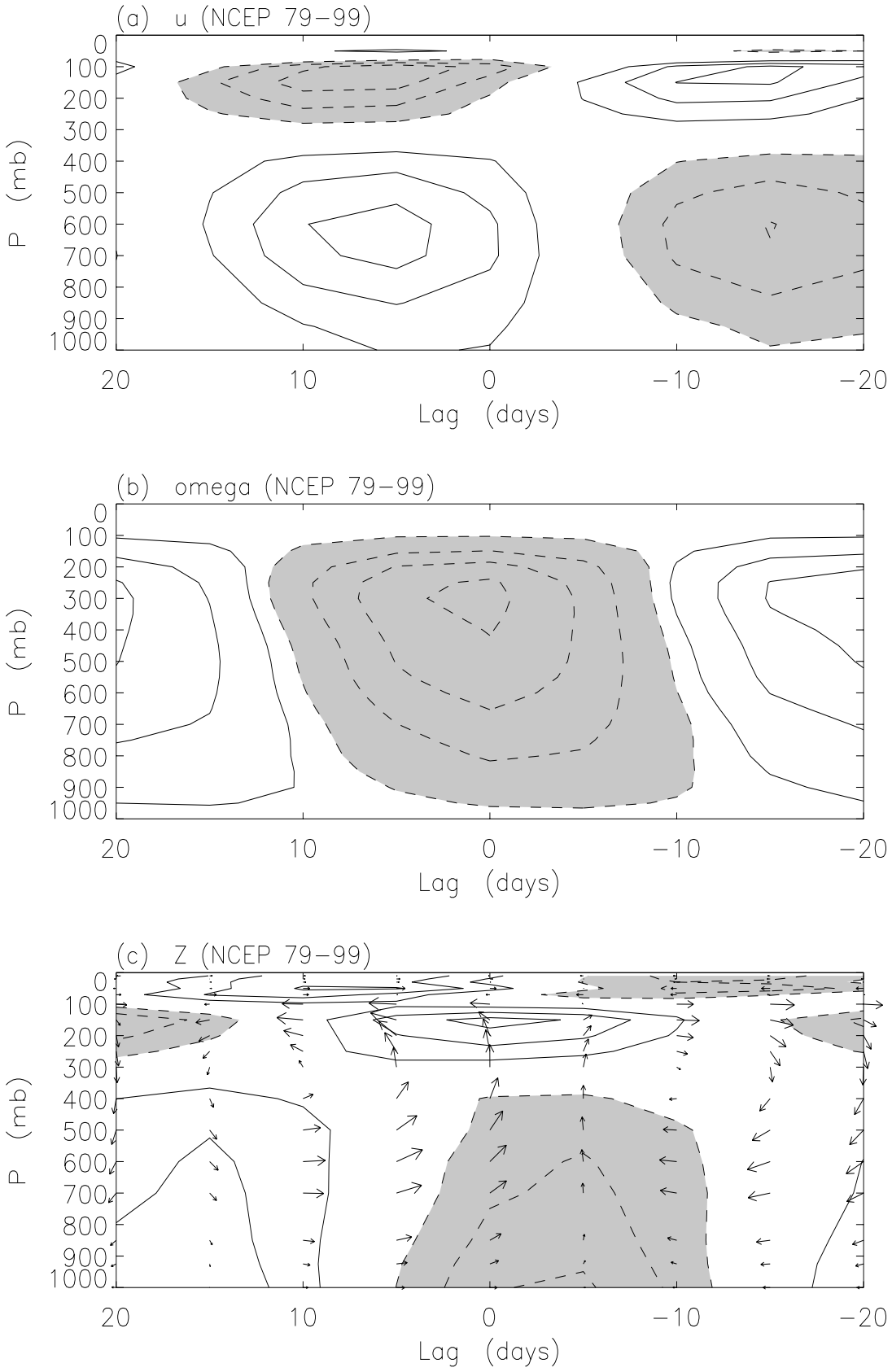
(a) u (NCEP 79−99)
P (mb)
0
100
200
300
400
500
600
700
800
900
1000
20
10
0
−10
−20
Lag (days)
(b) omega (NCEP 79−99)
P (mb)
0
100
200
300
400
500
600
700
800
900
1000
20
10
0
−10
−20
Lag (days)
(c) Z (NCEP 79−99)
P (mb)
0
100
200
300
400
500
600
700
800
900
1000
20
10
0
−10
−20
Lag (days)

Figure 3:

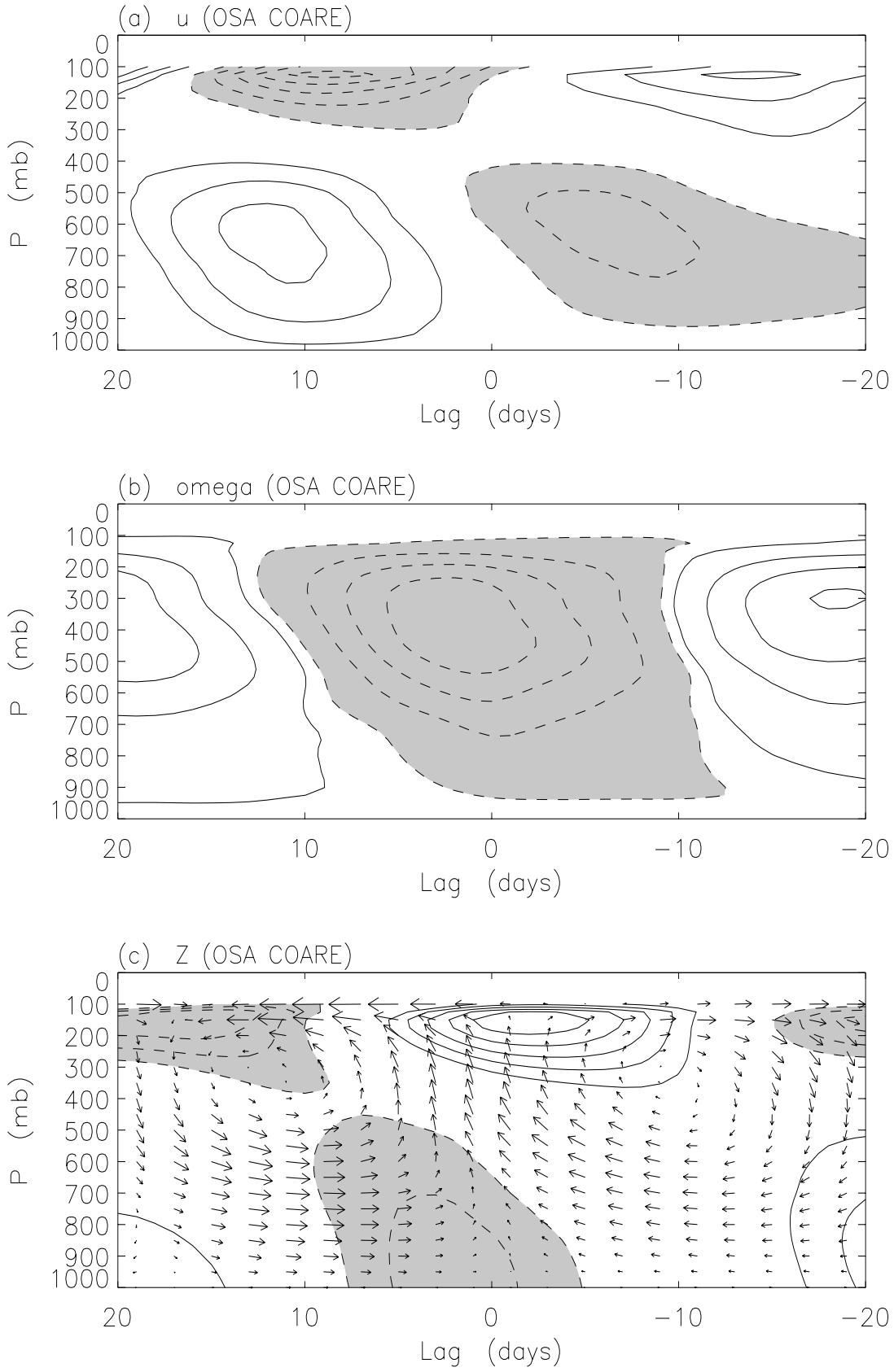
(a) u (OSA COARE)
P (mb)
0
100
200
300
400
500
600
700
800
900
1000
20
10
0
−10
−20
Lag (days)
(b) omega (OSA COARE)
P (mb)
0
100
200
300
400
500
600
700
800
900
1000
20
10
0
−10
−20
Lag (days)
(c) Z (OSA COARE)
P (mb)
0
100
200
300
400
500
600
700
800
900
1000
20
10
0
−10
−20
Lag (days)

Figure 4:

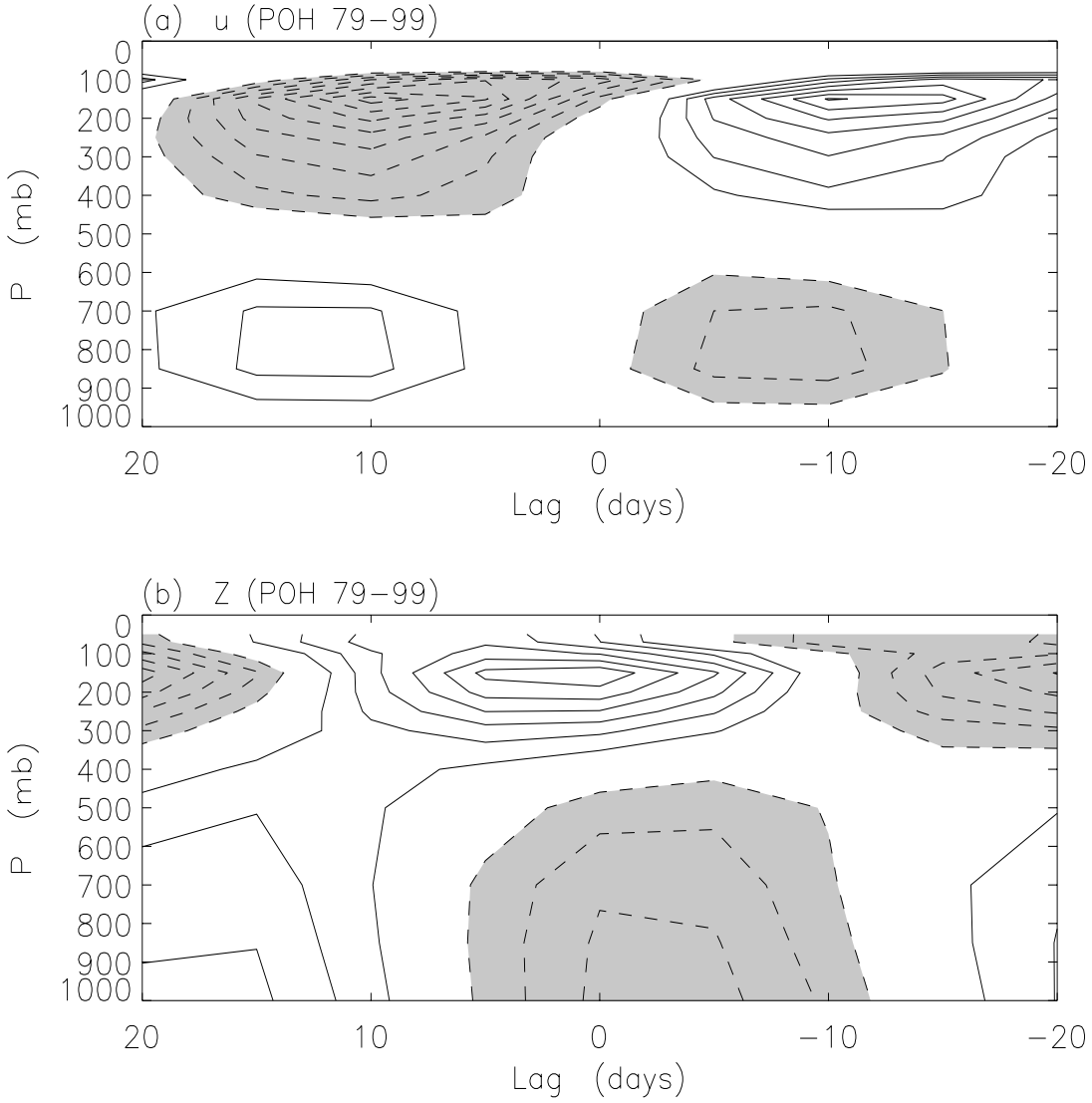
(a) u (POH 79−99)
P (mb)
0
100
200
300
400
500
600
700
800
900
1000
20
10
0
−10
−20
Lag (days)
(b) Z (POH 79−99)
P (mb)
0
100
200
300
400
500
600
700
800
900
1000
20
10
0
−10
−20
Lag (days)

Figure 5:

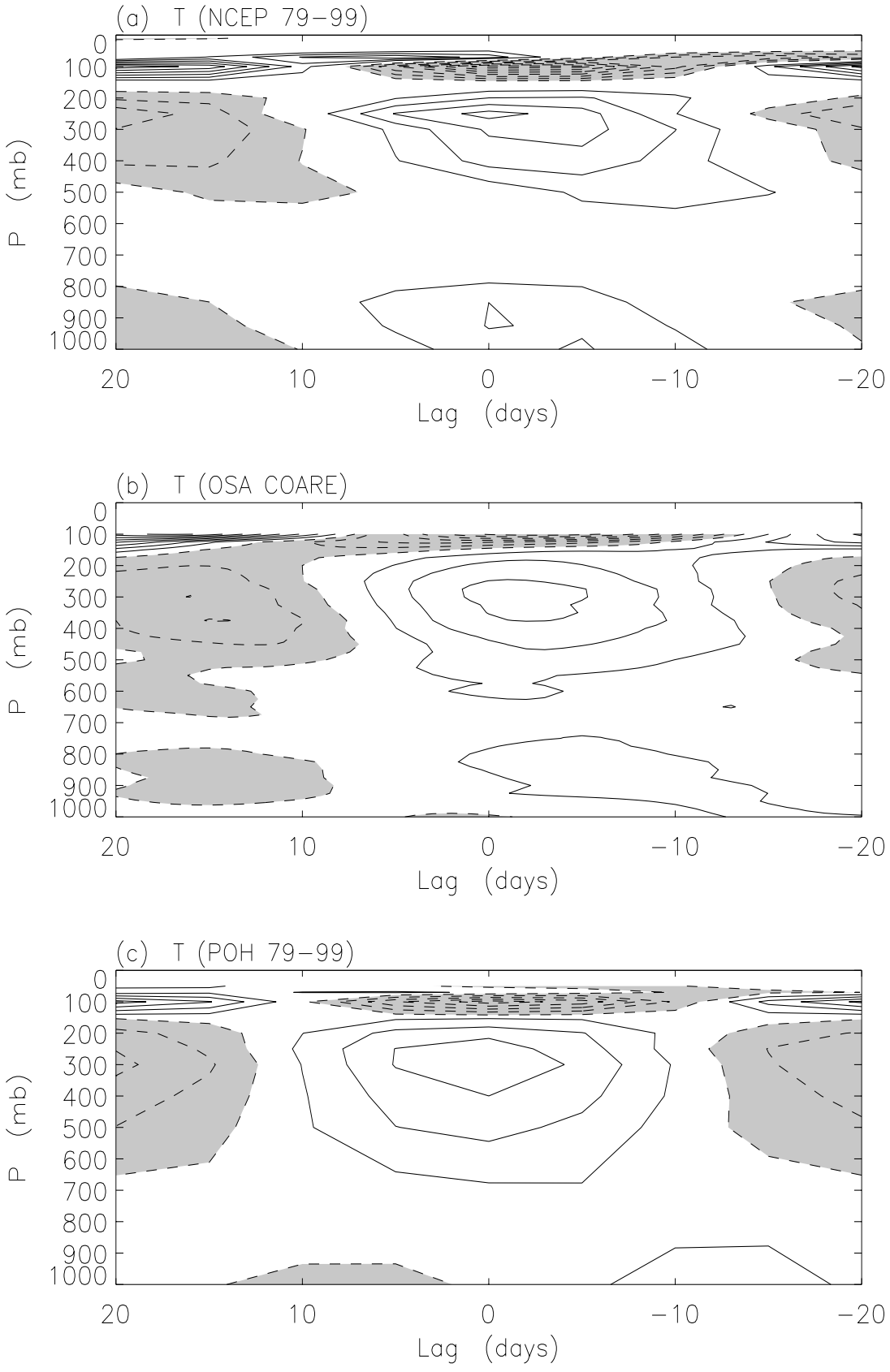
(a) T (NCEP 79−99)
(b) T (OSA COARE)
(c) T (POH 79−99)
P (mb)
0
100
200
300
400
500
600
700
800
900
1000
20
10
0
−10
−20
Lag (days)

Figure 6:

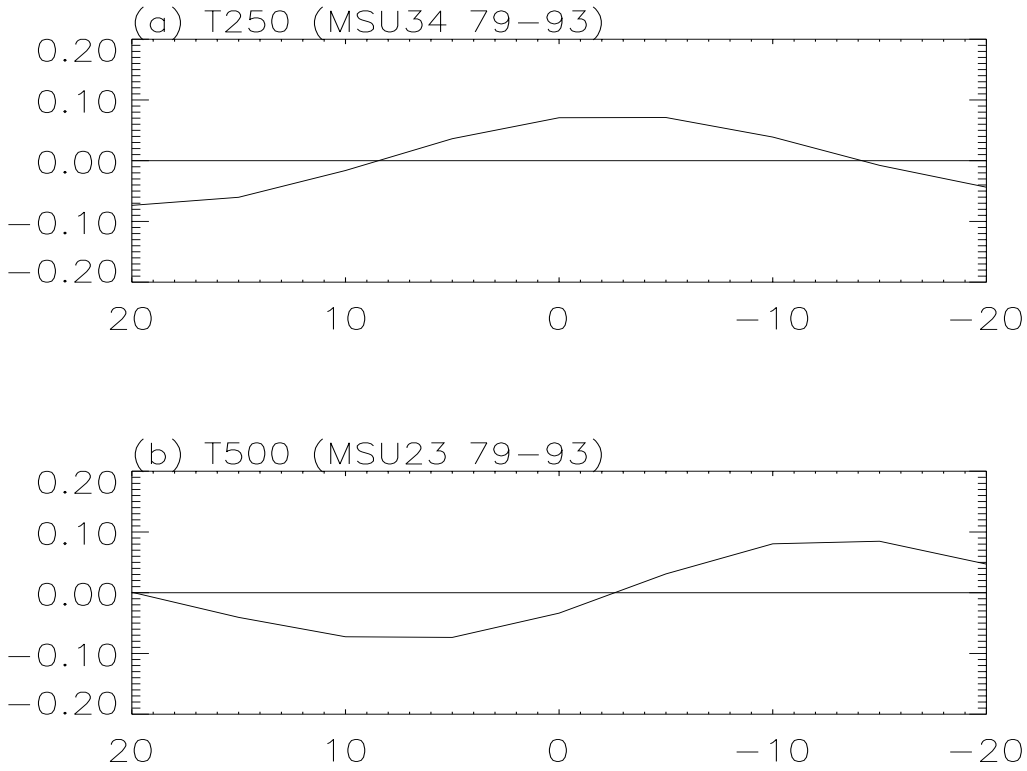
(a) T250 (MSU34 79−93)
0.20
0.10
0.00
−0.10
−0.20
20
10
0
−10
−20
(b) T500 (MSU23 79−93)
0.20
0.10
0.00
−0.10
−0.20
20
10
0
−10
−20

Figure 7:

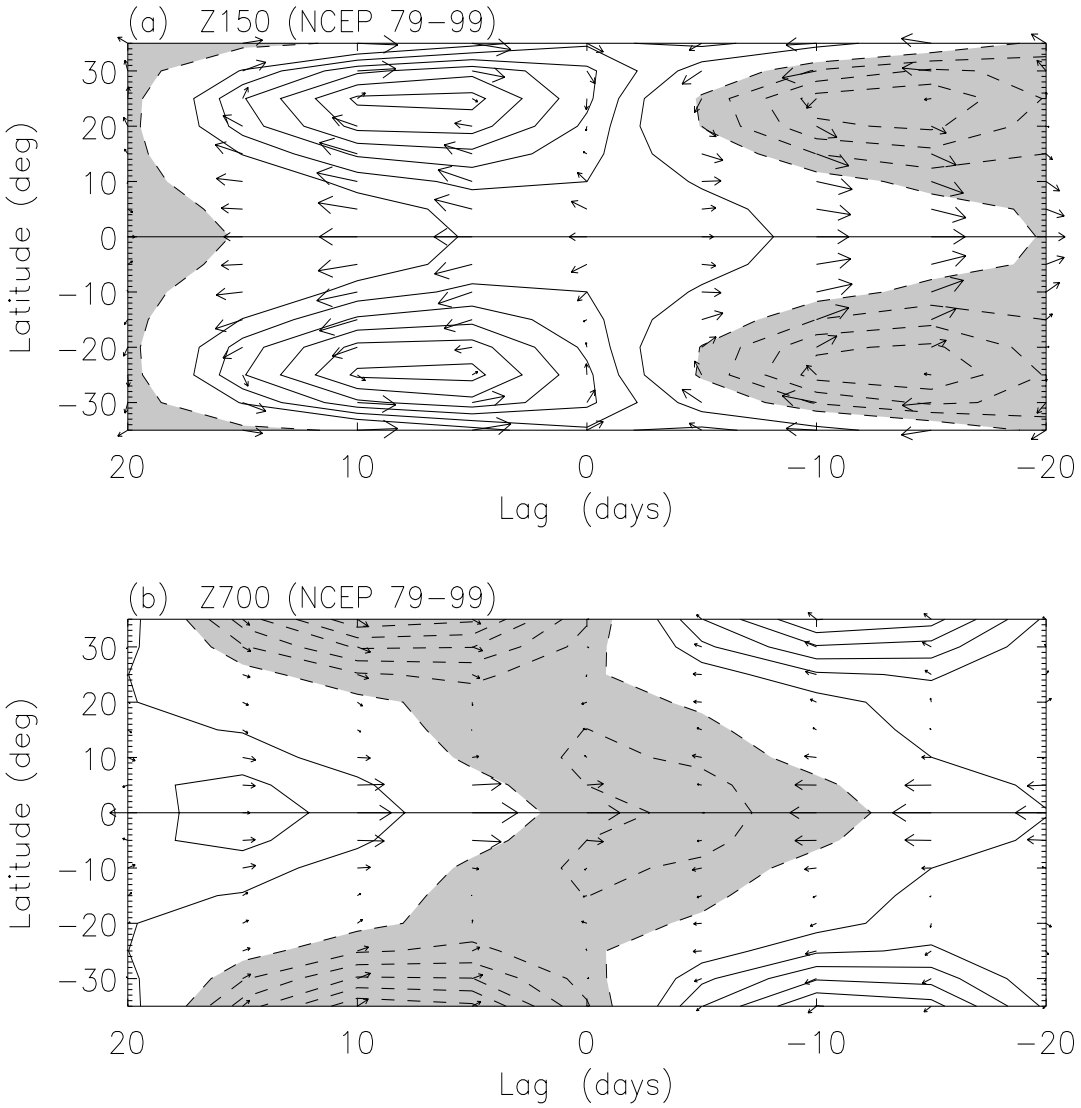
(a) Z150 (NCEP 79−99)
Latitude (deg)
30
20
10
0
−10
−20
−30
20
10
0
−10
−20
Lag (days)
(b) Z700 (NCEP 79−99)
Latitude (deg)
30
20
10
0
−10
−20
−30
20
10
0
−10
−20
Lag (days)

Figure 8:

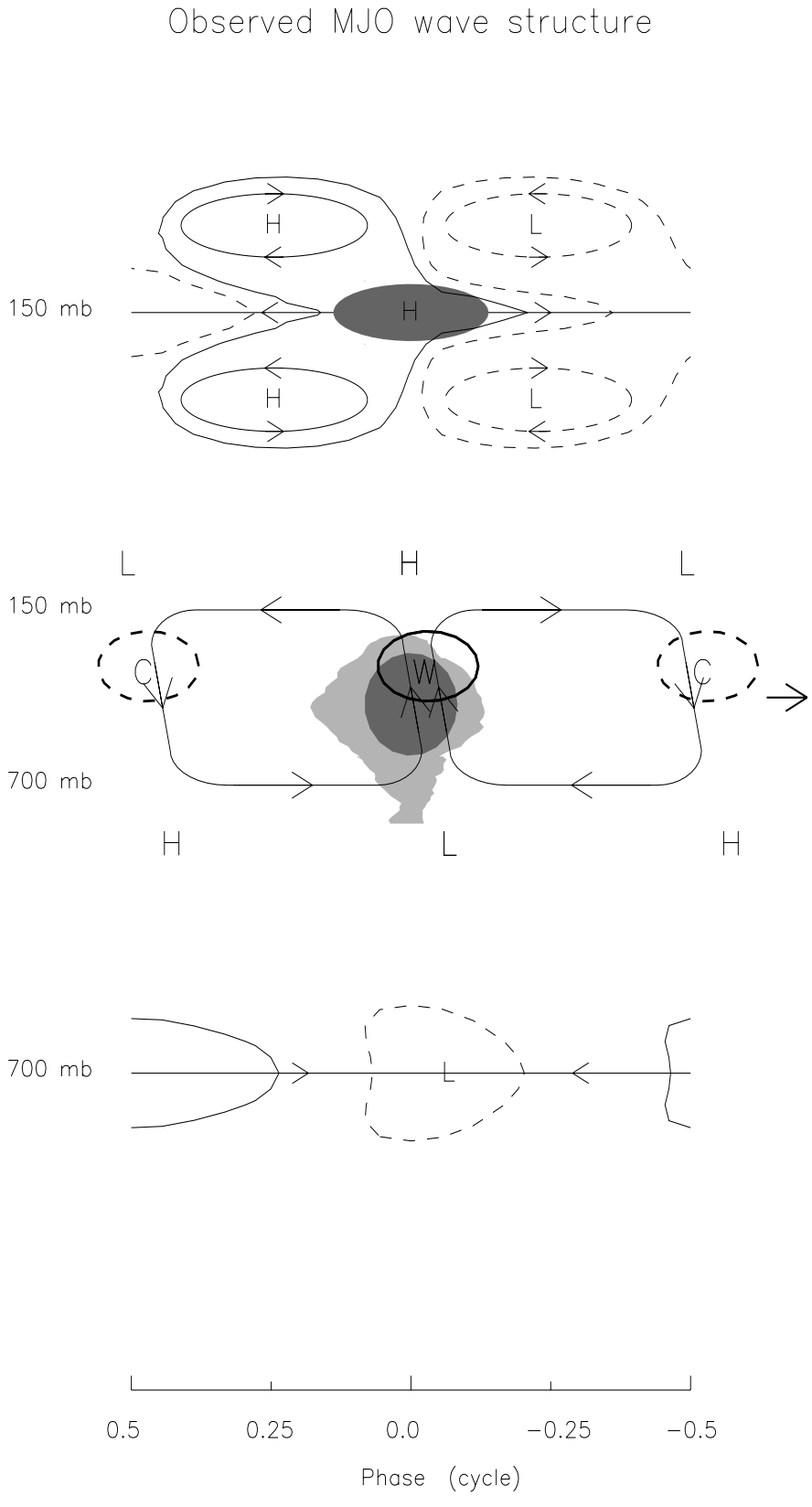
Observed MJO wave structure
150 mb
H
L
H
H
L
L
H
L
150 mb
C
W
C
700 mb
H
L
H
700 mb
L
0.5
0.25
0.0
−0.25
−0.5
Phase (cycle)

Figure 9:

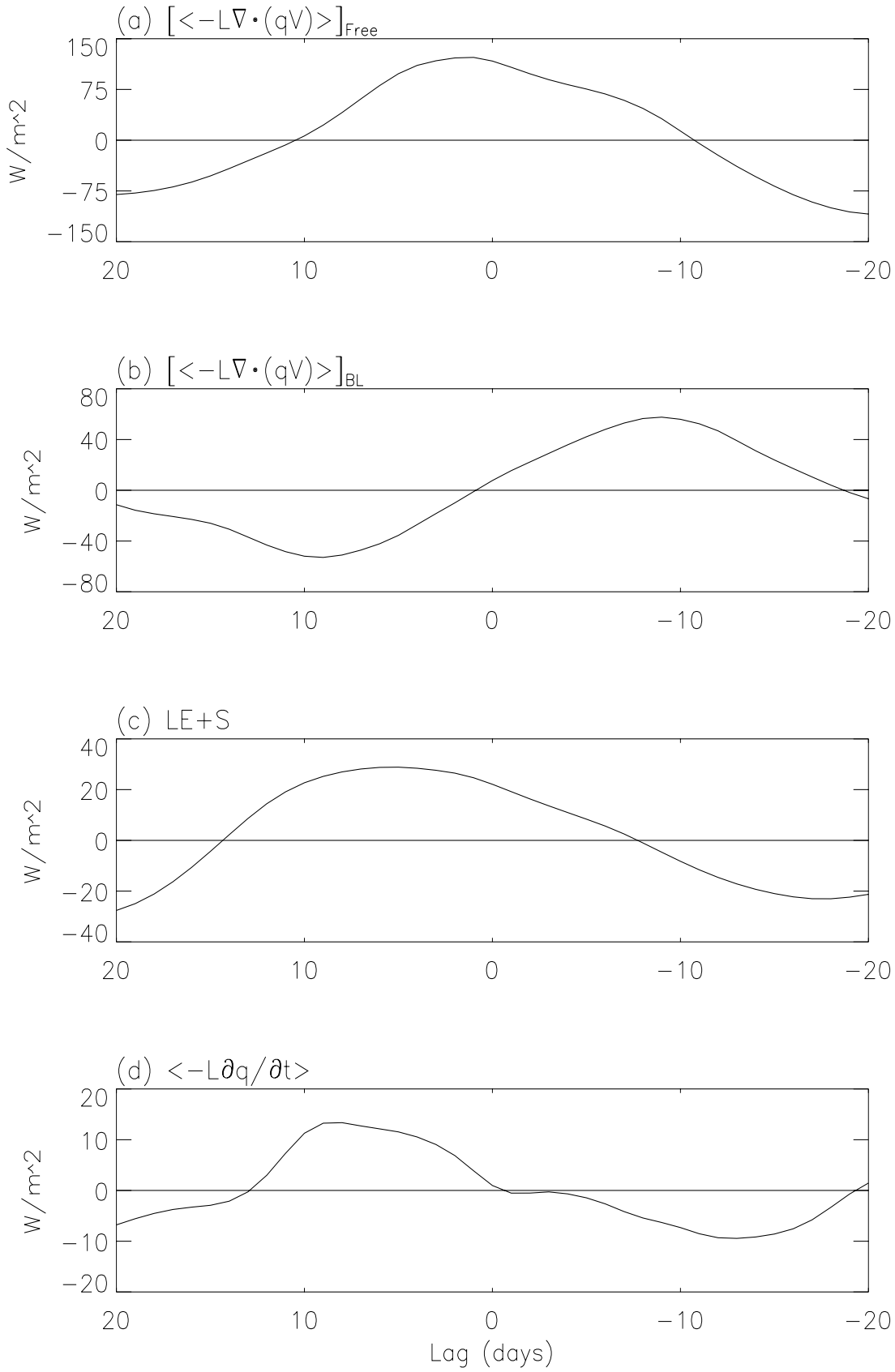
(a) [<−L∇•(qV)>]Free
150
75
0
−75
−150
W/m^2
20
10
0
−10
−20
(b) [<−L∇•(qV)>]BL
80
40
0
−40
−80
W/m^2
20
10
0
−10
−20
(c) LE+S
40
20
0
−20
−40
W/m^2
20
10
0
−10
−20
(d) <−L∂q/∂t>
20
10
0
−10
−20
W/m^2
20
10
0
−10
−20
Lag (days)

Figure 10:

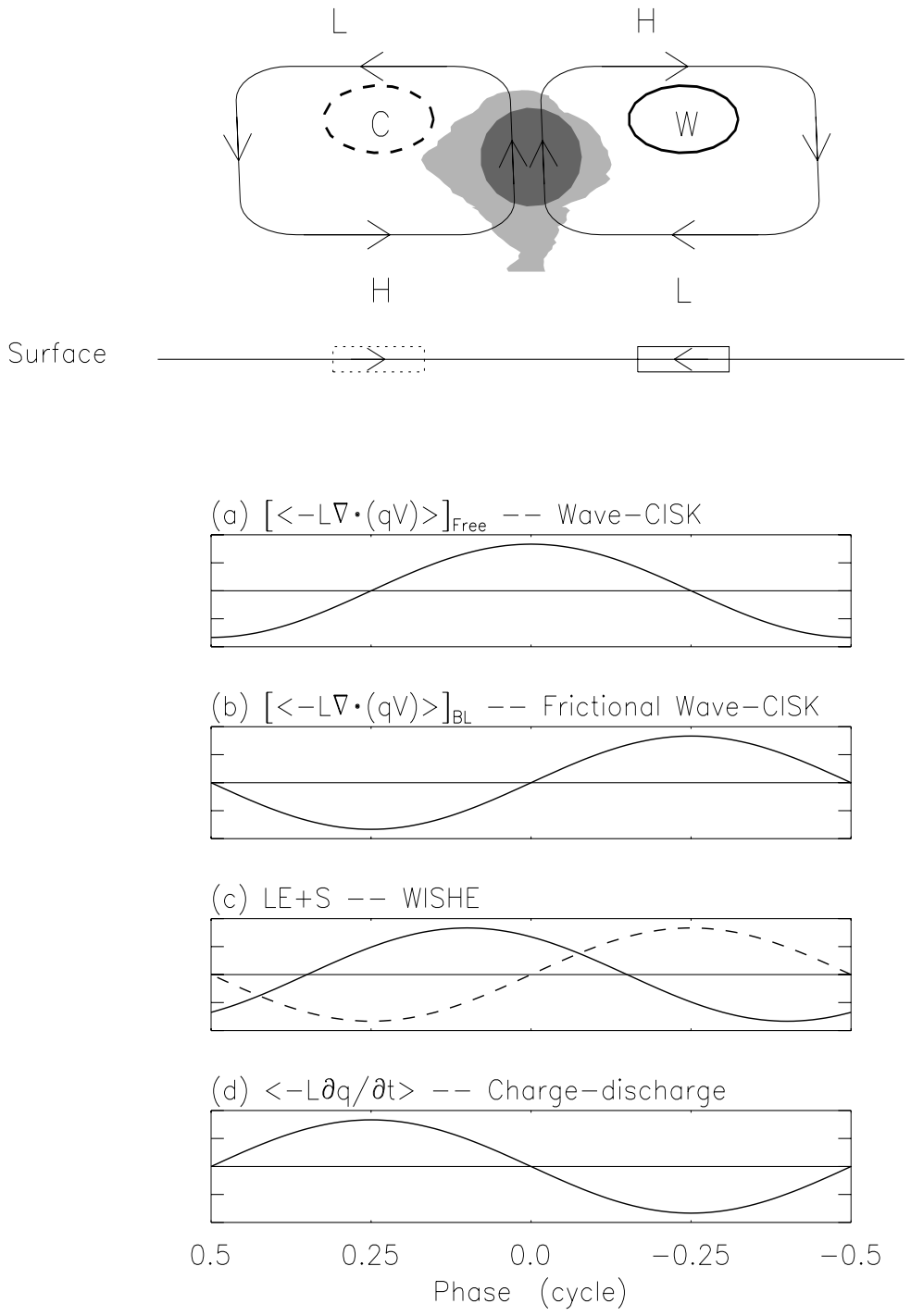
Wave−convection feedback in theoretical Kelvin wave
L
H
C
W
H
L
Surface
(a) [<−L∇•(qV)>]Free −− Wave−CISK
(b) [<−L∇•(qV)>]BL −− Frictional Wave−CISK
(c) LE+S −− WISHE
(d) <−L∂q/∂t> −− Charge−discharge
0.5
0.25
0.0
−0.25
−0.5
Phase (cycle)

Figure 11:

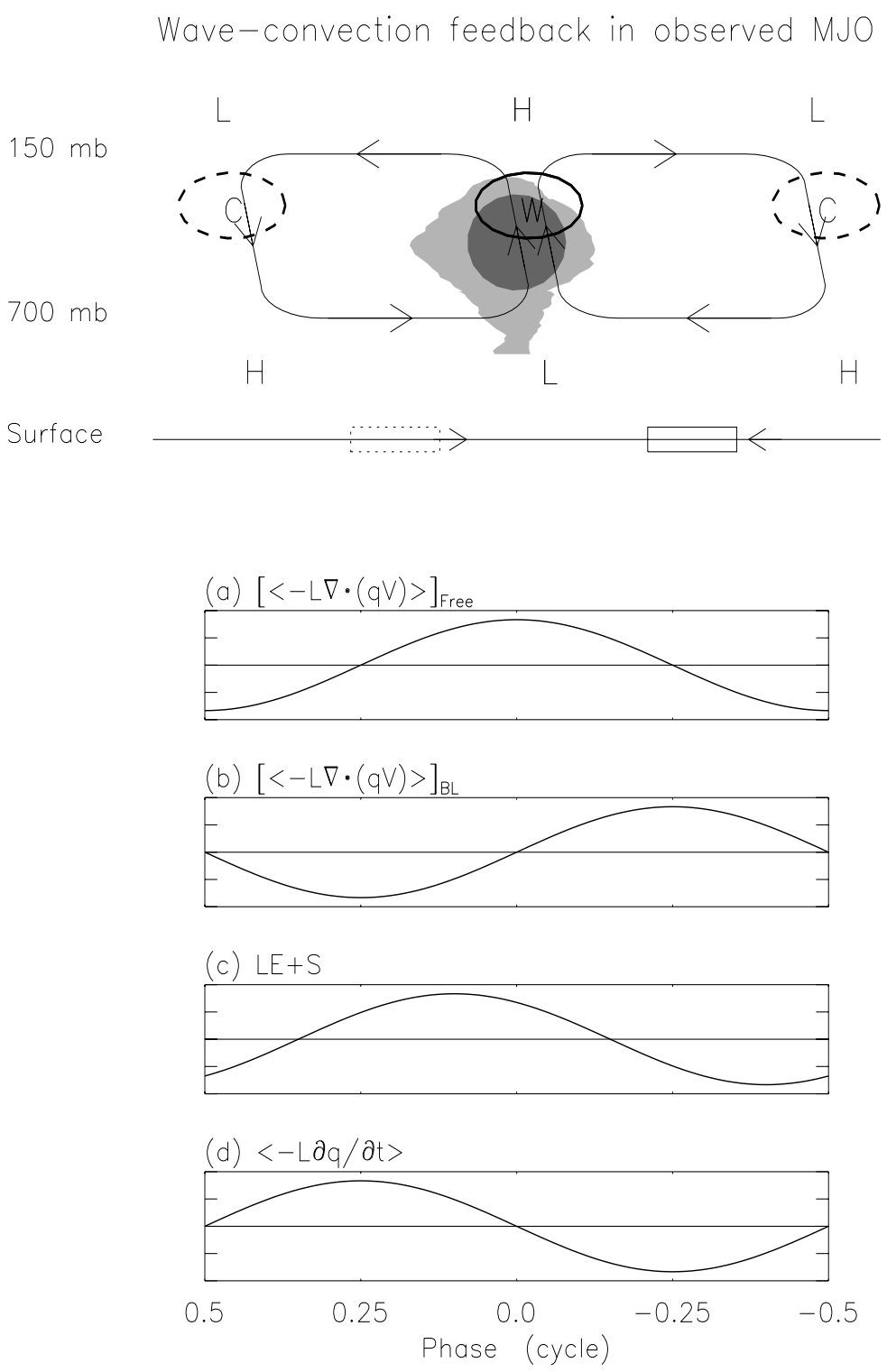
Wave−convection feedback in observed MJO
L
H
L
150 mb
C
W
C
700 mb
H
L
H
Surface
(a) [<−L∇•(qV)>]Free
(b) [<−L∇•(qV)>]BL
(c) LE+S
(d) <−L∂q/∂t>
0.5
0.25
0.0
−0.25
−0.5
Phase (cycle)

Figure 12: